

Multiwavelength study of Cygnus A I. Precession and slow jet speeds from radio observations

Katrien C. Steenbrugge^{1*} and Katherine M. Blundell²

¹*St John's College Research Centre, University of Oxford, St John's College, Oxford, OX1 3JP, UK*

²*University of Oxford, Department of Physics, Keble Road, Oxford, OX1 3RH, UK*

Accepted . Received

ABSTRACT

We study the jet and counterjet of the powerful classical double FR II radio galaxy Cygnus A as seen in the 5, 8 and 15-GHz radio bands using the highest spatial resolution and signal-to-noise archival data available. We demonstrate that the trace of the radio knots that delineate the jet and counterjet deviates from a straight line and that the inner parts can be satisfactorily fitted with the precession model of Hjellming & Johnston. The parameter values of the precession model fits are all plausible although the jet speed is rather low ($\lesssim 0.5c$) but, on investigation, found to be consistent with a number of other independent estimates of the jet speed in Cygnus A. We compare the masses and precession periods for sources with known precession and find that for the small number of AGN with precessing jets the precession periods are significantly longer than those for microquasars.

Key words: galaxies:active–galaxies:individual: Cygnus A–galaxies:jets.

1 INTRODUCTION

Cygnus A (3C 405), at a redshift of 0.05607 (Owen et al. 1997), is the closest powerful FR II classical double radio galaxy (see Fig. 1). At this distance, and for a Hubble constant of $73 \text{ km s}^{-1} \text{ Mpc}^{-1}$ (we also assume that $\Omega_M = 0.3$ and $\Omega_\Lambda = 0.7$), $1''$ corresponds to 0.9551 kpc, giving good physical resolution on its different structures and so Cygnus A has been well studied in the radio (e.g. Carilli et al. 1991).

In the nuclear region, a secondary point source has been identified by Canalizo et al. (2003) from a Keck II adaptive optics near-infrared image. The most likely explanation is that this is a remnant nucleus, due to a minor merger. In addition, redshifted H 21 cm absorption lines (Conway & Blanco 1995) and redshifted H₂ emission lines (Bellamy & Tadhunter 2004) are detected against the radio core, probably indicating the inflow of gas. A possible explanation is the infall of a giant molecular cloud, with the resultant radial gas motions fuelling the active galactic nucleus (AGN) and its jets and lobes (Bellamy & Tadhunter 2004). There is therefore quite some evidence for merger activity in this galaxy (Canalizo et al. 2003), although no large-scale structural disruption seems to have occurred (Owen et al. 1997). The galaxy is either part of the Cygnus A cluster or part of a cluster of galaxies falling toward this cluster (Ledlow et al. 2005). The latter scenario is supported by the fact that Cygnus A has a measured radial velocity offset of 2197 km s^{-1} from the mean cluster velocity (Ledlow et al. 2005).

In the optical, broadened (FWHM $500\text{--}990 \text{ km s}^{-1}$) emission lines (Tadhunter et al. 2003), as well as a blueshifted [O III] $\lambda 5007$

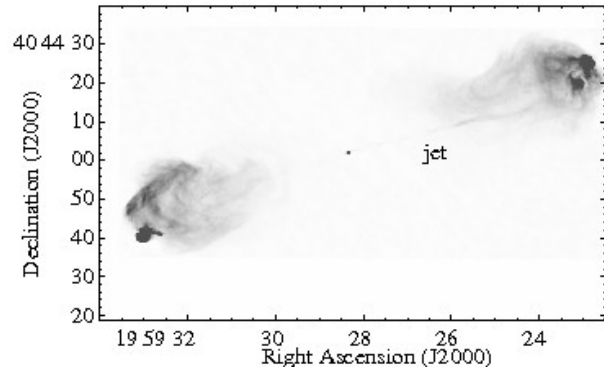


Figure 1. The image of Cygnus A at 5 GHz made by Chris Carilli using all four VLA configurations and first published in Carilli et al. (1991), showing the well known jet on the western, approaching side. Both lobes are brighter north of the jet trajectory.

line, are detected. The latter is identified as an outflowing, low velocity wind, as is commonly observed in the UV and X-ray spectra of Seyfert 1 galaxies.

In this paper we analyse three high spatial resolution radio data sets at 5, 8 and 15 GHz, to study the jet and counterjet in detail. In a companion paper (Steenbrugge et al. *in preparation*) we discuss the detection of a relic counterjet in a *Chandra* X-ray image. In a future paper we will discuss the relation between the lobes and present a detailed study of the X-ray spectral properties of the different brightness regions seen in the X-ray image. In the present paper, the different radio observations are described in Sect. 2, in Sect. 3 the

* E-mail: kcs@astro.ox.ac.uk

observational results are analysed, and interpretations are discussed in Sect. 4.

2 OBSERVATIONS

In our analysis we used three archival radio data sets. The 5-GHz radio data of Cygnus A (Fig. 1) were obtained by Chris Carilli using the A to D VLA¹ configurations (Carilli et al. 1991) and kindly given to us by him. In addition, we use the 8 GHz VLA A configuration data obtained by Carilli and which were published by Carilli et al. (1996) and Perley & Carilli (1996). The highest frequency band used was the 0.35'' resolution 15-GHz data made and published by Carilli et al. (1996), again using all four configurations of the VLA. The data were reduced by him, using standard procedures in AIPS as described in the above papers, and have undergone no further processing by us.

3 RESULTS

We first describe some of the details of the fine structure in the radio images. A preliminary study of the trajectory of the jet and counterjet was reported by Steenbrugge & Blundell (2007). Throughout this paper when referring to Cygnus A we reserve the terms jet and counterjet to refer to the western (approaching) and eastern (receding) sides respectively.

3.1 Inner radio jet

We define the inner jet as the portion of the jet that is closer to the core than the lobe is, i.e. where there is less likely to be an interaction of the back-flowing lobe material with the jet. We denote in Figs. 2 and 3 W1 to W6 to represent the inner jet, and E1 and E2 in Fig. 4 the inner counterjet, where E2 lies close to the inner edge of the counterlobe. In the 5- and 8-GHz images both the inner jet and the inner counterjet are observed. Both the jet and counterjet consist of knots, with seemingly smooth emission between some of the inner knots only detected in the 5-GHz image. In the 15-GHz image only the bright knot at the inner edge of the lobe, E2, is seen for the counterjet; however, for the jet there are 5 knots interior to the 5-GHz lobe (which are labelled W1 to W5 in Fig. 3). The inner jet and counterjet appear straight, and have a maximum offset angle between knot W3 and W4 and the nucleus of $1^{\circ}04' \pm 26'$. This possible offset is best observed in the 15 GHz data (Fig. 3), in which the knots are more sharply delineated, but is consistent with the 5- and 8-GHz images. No such detailed information can be obtained for the inner counterjet, which is significantly weaker in the 5- and 8-GHz images and not detected in the 15-GHz image. The inner counterjet is at an angle of 182.79 ± 1.5 degree to the western jet. The large error bar, compared to the offset of the knots in the jet, is due to the much weaker emission from the counterjet, which means only 2 knots are detected for the counterjet in the 5- and 8-GHz images.

3.2 Outer radio jets

We define the outer jets as that portion of the jets that clearly propagate through lobe plasma. The outer jet starts at W7 (see Fig. 2)

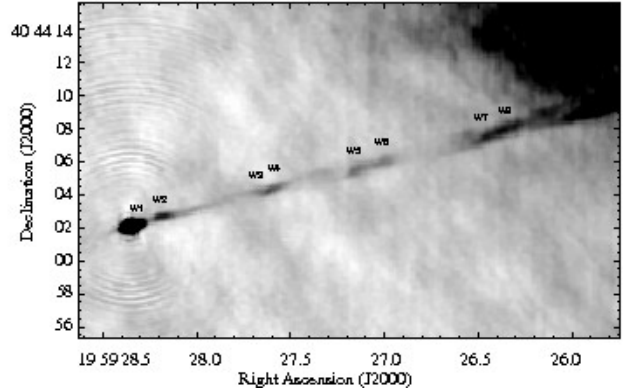


Figure 2. The inner jet of Cygnus A observed at 5 GHz. Note the weak emission between W1 and W2 which extends about half way to W3. Thereafter, there are only hints of smooth emission between the jet knots, which become brighter from W7 onwards. The jet seems straight, but note the possible bend between W3 and W4. W7 and W8 are the first jet knots in what we call the ‘outer jet’.

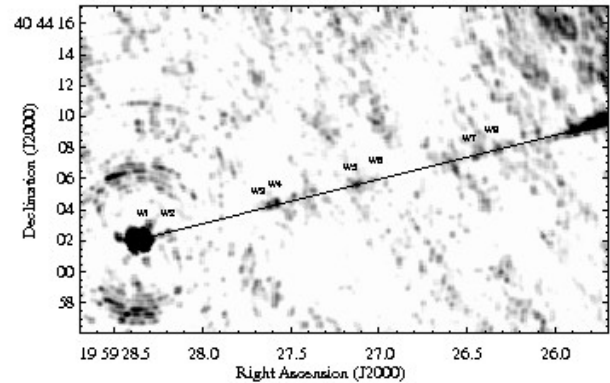


Figure 3. Detail of the inner jet of Cygnus A as observed at 15 GHz. The jet knots up to W6 are part of the inner jet. The inner edge of the 5-GHz lobe is just before W7. Note that the straight line drawn does not go through the centre of W4. The angle between the straight line drawn, the nucleus and the centre of W4 is $1^{\circ}04'$.

and the counterjet is represented by E3 to E8 (see Figs. 4 and 6). In Cygnus A the western lobe is much more prominent to the north of the jet; this is the case in all three radio bands studied. This allows us to trace the jet well “inside” the lobe. Also the eastern lobe is distributed asymmetrically around the counterjet in the same sense, i.e. there is a preponderance of emission to the north (this is seen most clearly at 15-GHz, see Fig. 6), allowing us to observe the counterjet all the way to a hotspot. We observe that the jet bifurcates or “threads” just inside the inner edge of the lobe (between W10 and W11 in Fig. 5). Furthermore, the bends in the outer jet are more easily observed than in the inner jet, and were first noticed by Carilli et al. (1996). Interestingly, the angle between W9 and W12 (see Fig. 5) is $1^{\circ}33' \pm 10'$, very similar to the angle determined between knot W3 and W4 in the inner jet. Further evidence that the jet bends is that if we extend the inner jet to the hotspots (the extended jet line shown in Fig. 5), it does not terminate in either one of the 2 brighter hotspots or even the third weaker hotspot. The difference in angle

¹ The Very Large Array is a facility of the National Radio Astronomy Observatory, National Science Foundation

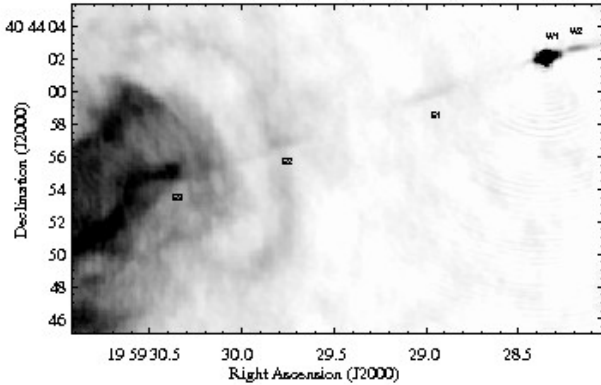


Figure 4. Detail of the inner counterjet of Cygnus A as observed at 5 GHz. Note how the jet knots are much weaker than on the jet side. The inner edge of the counterlobe does show very interesting features, such as the rather weak “ring” (which appears to surround E2) and the two “antennae”(at E3).

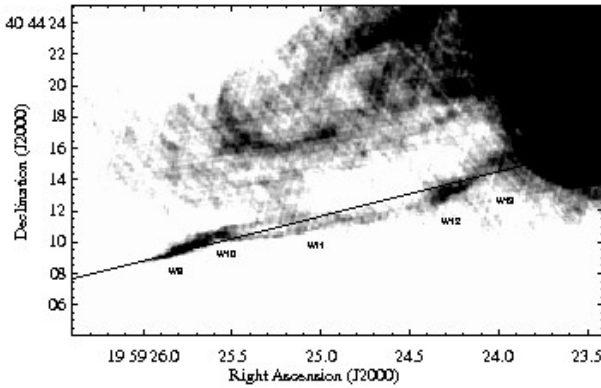


Figure 5. Detail of part of the outer jet near the western lobe, observed at 8 GHz. The thin solid line indicates the direction of the inner jet. Note how the jet bifurcates between W10 and W11, a phenomenon known as threading. This figure clearly shows the bending of the jet between W9 and W12.

between the extended jet line and a line from the radio core to the middle of the inner bright hot spot is $\sim 2^\circ 30'$.

We do not observe the counterjet to thread in the same way the jet does, but we do observe two bright knots which indicate that the counterjet clearly bends (see Fig. 6). The angle subtended at the nucleus by the 2 small knots E4 and E5 is only $40' \pm 11'$. However, unlike the jet which seems to bend around the extended jet line shown in Fig. 5, these 2 knots seem to be placed where the counterjet starts to bend through a large angle. The remaining knots are only detected at 15 GHz, as the lobe emission dominates in the other bands. The angle between the nucleus, and the E4 and E6 bright knots is already $3^\circ 33' \pm 10'$, and replacing E7 for E6 the angle is $6^\circ 18' \pm 8'$. The jet bends by an angle of $\sim 27^\circ 31'$ between the nucleus, E4 and E9, the weaker of the two hotspots on this side of the source. The width of jet knot E8 in the 15-GHz image is $\sim 2'' .9$.

3.3 The relic counterjet observed in X-rays

In a companion paper (Steenbrugge, Blundell & Duffy) we describe a relic counterjet in Cygnus A which is revealed by deep *Chandra*

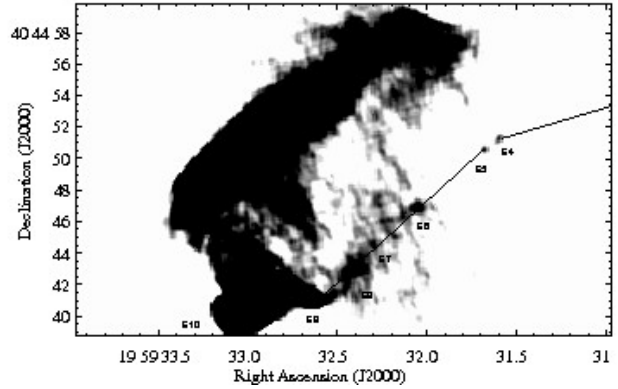


Figure 6. Detail of the outer counterjet (whose knots are labelled E4 to E8) and the eastern hotspots (E9 and E10) observed at 15 GHz. Due to a lack of southern lobe emission in this band, we can follow the counterjet all the way to the hotspot region. The 2 solid lines indicate the direction of the counterjet, which changes direction between knots E4 and E5.

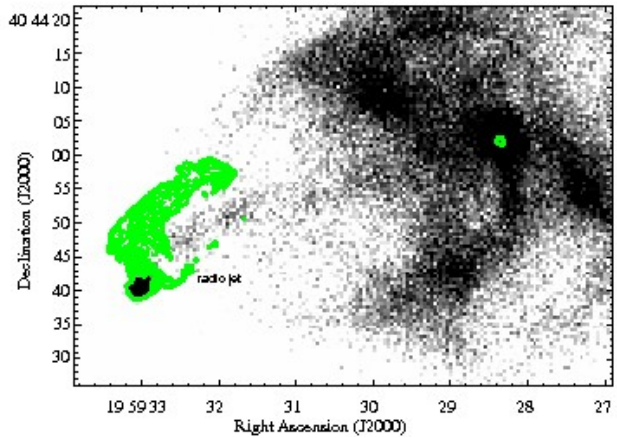


Figure 7. Detail of the *Chandra* 200 ks co-added ACIS-I image with a transfer function optimised to show the relic X-ray counterjet. The contours are from the 15 GHz image, indicating the flux between 0.008 and 0.05 Jy. Note how the transversely extended X-ray counterjet goes through a low luminosity radio region, seemingly pushing radio lobe plasma north. Furthermore, note that the radio counterjet is detected to the south of the X-ray counterjet.

X-ray imaging. In that paper, we discuss how its broad, transverse appearance (compared with the diameter of radio jets in this object) arises because of expansion. Fig. 7 shows where the relic X-ray counterjet lies in relation to the most prominent northern 15-GHz lobe emission and to the current radio counterjet. We suggest that the expanding relic counterjet is pushing the lobe and current counterjet plasma radially outwards from its axis. This is a possible explanation for the $\sim 27^\circ 31'$ bend of the radio counterjet, which is not observed for the relic X-ray counterjet. Also the asymmetric luminosity of the counterlobe plasma, much brighter towards the north, can be explained in this manner.

4 DISCUSSION

4.1 Precession

In this section we consider precession of the jet axis as the origin of the deviations from a perfect straight line as traced by the knots forming the jet and counterjet of Cygnus A. Precession, of course, in its most general sense includes any change in the direction of the instantaneous spin axis. All examples of precession are fundamentally two-sided (applying to the emerging jet and counterjet equally and simultaneously in the rest-frame of the nucleus). Temporal variation in precession parameters, as long as two-sided and instigated at the jet launch point by angular momentum changes (e.g. caused by variation in the fuelling), are properly described as precession and are distinct from Scheuer's Dentist's Drill phenomenon (Scheuer 1982). This phenomenon is a response of a jet, on *one side* of a source, to local conditions (for example, buoyancy effects corresponding to local motions or inhomogeneities); we note that dentists' drills are one-sided. Although the dentists' drill could work for both sides of the jet, as the effect is environment dependent, one would not expect a symmetric pattern.

Here we investigate whether sustained periodic precession is a plausible explanation for the curvature seen in Cygnus A's jets. Sustained periodic precession is famously exhibited by the jet axis of the Galactic microquasar SS 433, which has a relatively rapid precession period of ~ 162 days. A geometric model describing the precession of the jet axis in this, or any similarly behaving object, is presented by Hjellming & Johnston (1981). In this model, symmetric jets are launched at speed β along an axis which traces a cone throughout a precession period P , of opening angle ψ inclined to our line of sight at angle i , in terms of a precession phase ϕ . The jet material, once launched, is assumed move ballistically, i.e. suffer no acceleration or deceleration.

Reasonable fits to the curvature of the jets in Cygnus A can be obtained with the following parameter values: a cone opening angle of $1^\circ \pm 0.30^\circ$, an angle between this cone axis and our line of sight of $60^\circ \pm 5^\circ$, and an angle of the cone axis projected on the plane of the sky with respect to the East-West line of $14.7^\circ \pm 1^\circ$. D is determined by the redshift 0.05607 for the cosmology assumed in this paper, and is not considered to be a free parameter. The characteristic angular periodicity of the appearance on the sky of a precessing jet is determined by $\beta P/D$ (where D is the distance of the precessing jet from Earth). Different values of P and D will cause a simple magnifying effect on this angular scale, but higher values of β will introduce asymmetric curvature on the opposite sides due to increasing asymmetric light-travel time effects.

The projection of a precessing jet with these parameters for particular related values of β and P are shown for the 5 GHz jet in Fig. 8 and for the 15 GHz counterjet in Fig. 9. The fit was made to the 15 GHz image and has values: $\beta = 0.35 c$, $P = 10^8$ days (or 0.274 Myr), a line of sight angle of 60° and a cone opening angle of 1° . The allowed pairs of β and P that give a decent fit range between: $\beta = 0.3 c$ and $P = 1.17 \times 10^8$ days to $\beta = 0.5 c$ and $P = 0.7 \times 10^8$ days. To quantify the goodness of the precession model we traced the jet by-eye and calculated the standard deviation between the precession model fit and the by-eye fit. For both Right Ascension and Declination we use proper arcseconds. We then vector added those standard deviations and obtained a difference between our best fit precession model and the by eye fit of $0.072''$ (proper arcsec). For a fit with $\beta = 0.5$ this value worsens to $0.080''$, and for $\beta = 0.25$ this value is $0.086''$. An opening angle of 1.4° worsens this value to $0.079''$. A line of sight angle of

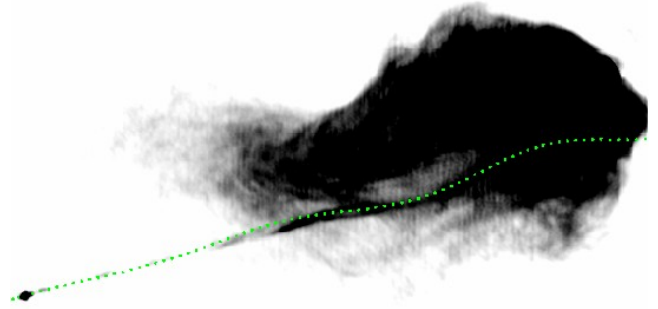


Figure 8. 5-GHz image of the jet side of Cygnus A, with the best fit precession model as fitted to 15 GHz overlaid as green dots. The jet knots are launched anti-parallel along a jet axis which precesses, tracing out a cone of opening angle 1° . Details of parameters for the precession model fitted are listed in the text.

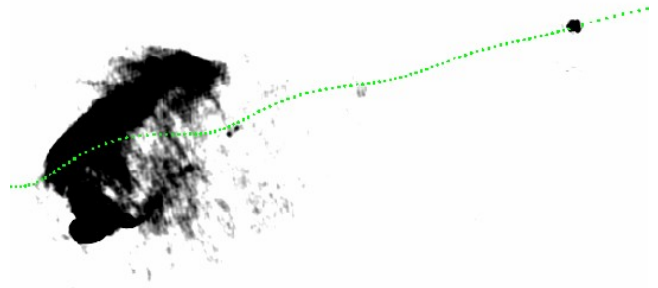


Figure 9. 15-GHz image of the counterjet side of Cygnus A, with the best fit precession model overlaid as green dots. Note that the expansion of the relic counterjet (shown in Fig. 7) will push the counterjet to the south. Therefore, precession does not explain the $\sim 27^\circ 31'$ bend in the counterjet.

65° worsens the goodness of fit to $0.075''$. Finally, assuming no precession (i.e. a completely straight jet), the fit worsens to $0.103''$.

Thus, for the approaching jet shown in Fig. 8, a precessing jet axis gives encouraging results. It is particularly interesting that the range of jet speeds which work are consistent with the slower jet speeds inferred from an independent method and literature described in Sec 4.5 and 4.6. The fit to the counterjet is clearly poorer than the fit to the jet. However, allowing for a $\sim 1^\circ$ difference from the assumed 180° angle between the jets does lead to a much improved counterjet fit. The considerable change in angle ($\sim 27.5^\circ$) of the current radio counterjet seen in the east of Cygnus A occurring between E4 and E5 is unlikely to be due to precession, but could be influenced by the expansion of the relic counterjet (see Section 3.3). Actually, the precession fit obtained from fitting the 15-GHz image goes surprisingly well through most of the relic X-ray counterjet (Steenbrugge, Blundell & Duffy, companion paper), as shown in Fig. 10. Although the fit is poor at the outer part of the relic X-ray counterjet, the decent fit for part of the jet suggests that precession has been fairly constant for different jet episodes, considering that the precession phase likely was different.

We remark that if the jet knots move at speeds $\sim 0.3 c$, a rather low value for the jet speed, that the time taken to reach the current location of the hotspots is $\sim 10^6$ years.

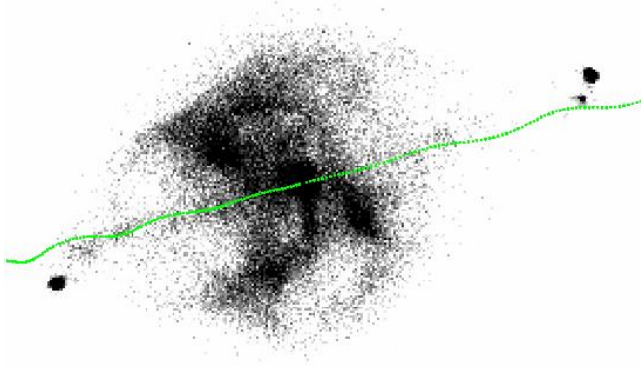


Figure 10. The 200 ks image of Cygnus A (Steenbrugge, Blundell & Duffy companion paper), with the precession model fitted to the 15-GHz image and shown in Figs. 8 and 9 overlaid as green dots.

4.2 Other models for jet bending

We will briefly review some of the other models that in the past have been proposed to explain bending of jets or tails and suggest why they are unlikely to apply to Cygnus A.

A possible mechanism for jet bending, that can easily be excluded for Cygnus A, is the bending due to the orbiting of the black hole within its galaxy. For an orbiting object the jet curvature is plane symmetric, thus the bend in the jet and counterjet are towards the same side. Whereas in precession, the jets are point symmetric (at least for slow speeds), i.e. the bends have a 180° mirror on the other side. The curvature of Cygnus A's jets is consistent with point symmetry (see Fig. 8 and 9).

Eilek et al. (1984), studying the wide-angle tailed source 3C 465, tried several models to explain the C-symmetric, i.e. mirror symmetric, bending of its outer jets. As the jets of 3C 465 inside the host galaxy are straight, all models ascribe the effect to the intra-cluster medium (ICM). Although no model appeared convincing to those authors, the most likely model is that the bending is due to the large-scale velocity of magnetic fields in the ICM. 3C 465 is in the centre of a cluster, therefore it likely has no large-scale velocity of its own to explain the bending. The bending in the outer jet of Cygnus A is outside the host galaxy, and Cygnus A is either part of a group or a cluster. However, large-scale velocity or magnetic field structure would also bend the lobe, and this is not observed. The fact that in Cygnus A the bending reverses (first away from the straight line in Fig. 5 and then back again), would require highly ordered fields on rather small scale and with a very specific configuration. Finally, this explanation cannot explain the subtle bending of the inner jet.

A third model proposed by Wirth et al. (1982) is that the gravitational potential of a companion galaxy torques and thereby bends the jet. Wirth et al. (1982) use this model to explain the jet shape in the dumbbell galaxy NGC 326, which Gower et al. (1982) modelled as precession. Wirth et al. (1982) assume that in NGC 326 only the inner part of the jet is a current jet, and that the more extended emission is from a previous jet episode. This is an unlikely explanation for the bending of the jets in Cygnus A, as the galaxy, although in either a group or a cluster, does not have a very close companion of similar mass like the dumbbell galaxy of NGC 326. Furthermore, the scale over which the jet bends is such that the companion should have a rotation period of less than the inferred precession period (of the order 3×10^5 years), for the range of jet

speeds inferred in Sect. 4.1. For a companion galaxy at 20 kpc distance this would require an orbital speed close $0.1 c$, an implausibly high value.

Finally, it is possible that gas pressure within the host galaxy itself, due to the host galaxy rotation, bends the jet. As the rotation speed is a function of radius in the galaxy, a very efficient, i.e. near instantaneous, transfer of angular momentum of the gas to the jet, could cause the jet to first bend in one direction and then turn back again. Namely, the jet would be rotating too fast for the radius at which it finds itself after travelling further out. In this model, once the jet leaves the host galaxy, or the gas pressure is too low, the jet would travel in a straight line. To explain the bend in the outer jet, which is well outside the host galaxy, one needs to postulate that the jet speed changed over time. As a result the amount of bending, and thus the angle from which the jet left the host galaxy varies with time. Although this remains to be explored in detail, an argument against this possibility is that the angle over which the inner and outer jet bend is (within errors) the same, which would be unlikely if the bending is caused by two different processes.

4.3 Comparison of precession period with other sources

In this section we compare the results from our precession model (Sec. 4.1) with the results for precessing jets that are available in the literature. For most objects the mass is not yet determined. Therefore we deemed that the young stellar objects have a mass of $1 M_\odot$, the microquasars of $7 M_\odot$ and the AGN of $10^8 M_\odot$, unless there was a value in the literature. (Considering the spread in mass for the objects considered, the uncertainty in mass is not too problematic.) Fig. 11 shows the relationship between mass and precession period for younger stellar objects, microquasars and AGN.

AGN clearly have longer precession periods than either microquasars or young stellar objects. Considering that microquasars are likely to be much better analogues of quasars than young stellar objects (e.g. because of the similarity of their jet speeds; the jet speeds of young stellar objects are only of order 100 km s^{-1}), it is interesting to note that the distribution of AGN points and that of the microquasars lie a similar distance below the $y = x$ line, drawn solely to guide the eye, and not a fit to the data. This may be an indication that precession periods in these objects increase with mass.

This possible correlation would disappear if additional data-points are located in either the bottom right or the top left corner of Fig. 11. The first of these would occur for AGN having very short precession periods. Fine angular resolution is necessary to be able to detect very short precession periods in distant AGN jets. There have been claims in the literature of very short precession periods in AGN, mostly from VLBI observations. For example, the 30.8-yr derived precession period in PKS 1830–211, which is a blazar with two nuclei (Nair et al. 2005). However, these short precession periods are most likely due to the orbital motion of the binary as explained and modelled by Kaastra & Roos (1992) and recently reviewed by Lobanov & Roland (2005). The difference in precession periods for microquasars and AGN should be confirmed by more data, especially better VLBI data to rule out precession of AGN on timescales of tens of years or less. The second of these would occur if Galactic microquasars are discovered to have very long precession periods. In general, the data available for young stellar objects and microquasars are not sensitive to precession periods longer than about a 1000 years. At present, we only know of one microquasar, SS433 embedded within the W50 nebula, with precessional information which can be traced back to $\sim 10^5$ years ago.

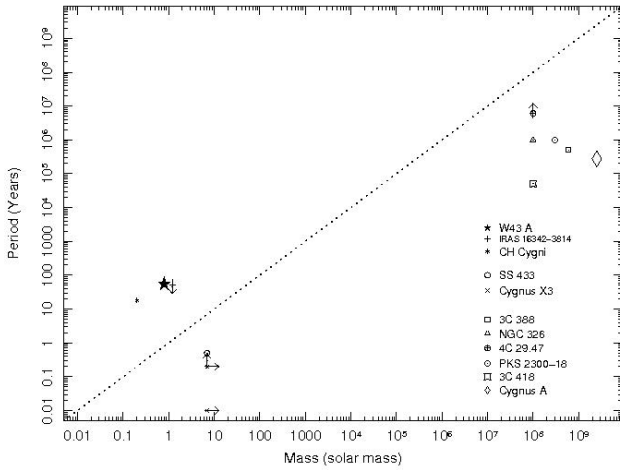


Figure 11. The plot shows the precession period and (estimated) mass for young stellar objects, microquasars and AGN showing evidence of precessing jets. The mass for those sources without a determined mass quoted in the literature was assumed as follows: for the young stellar objects $1 M_{\odot}$, for SS 433 and Cygnus X-1: $7 M_{\odot}$ and AGN $10^8 M_{\odot}$. References: W43A: Vlemmings et al. (2006), IRAS 16342–3814: Sahai et al. (2005), CH Cygni: Crocker et al. (2002), SS 433: Blundell & Bowler (2004), Cygnus X-3: long period and mass: Mioduszewski et al. (2001), short period: Miller-Jones et al. (2004), 3C 388 and NGC 326: Gower et al. (1982) for period, Woo & Urry (2002) for the mass of the former, 4C 29.47: Condon & Mitchell (1984), PKS 2300–18: Hunstead et al. (1984) for the period and Wu & Liu (2004) for the mass, 3C 418: Muxlow et al. (1984), Cygnus A: Tadhunter et al. (2003) for the mass, see this paper for the period. For Cygnus A the size of the symbol corresponds to the error bars in mass and period.

Interestingly, the microquasars have shorter precession periods (~ 162 days in the case of SS 433) compared to the young stellar objects (~ 50 years), although they are certainly more massive than the young stellar objects. (The uncertainty in the mass does not undermine this finding.) It is clear that more data points, and including neutron stars with precessing jets, would be very helpful in aiding our understanding of jet precession and the interpretation of Fig. 11.

4.4 Causes of precession

In the following, we detail three possible mechanisms for the precession observed in the jet. For all cases we assume that the jet is launched from the inner part of the accretion disc, but outside the warping radius. The Lense-Thirring effect will realign the angular momentum of the accretion disc within the warping radius, with that of the central black hole. All three mechanisms described involve creating a misalignment of the accretion disc, with either the black hole or the galactic stellar disc. Therefore the secure identification of precession in active galactic nuclei with a super-massive black hole would seem to indicate that the jet must be launched from the accretion disc and not the black hole.

4.4.1 Gas flow onto accretion disc

Gas, perhaps from a recent merger, channelling onto the accretion disc can cause a misalignment of the angular momentum vector of the accretion disc and the black hole. Redshifted HI 21-cm absorption (Conway & Blanco 1995) and redshifted H₂ emission

lines (Bellamy & Tadhunter 2004) are observed in the nucleus of Cygnus A, most likely indicating gas inflow. Therefore this is a possible mechanism for Cygnus A. The realignment of the accretion disc with the black hole was studied by Scheuer & Feiler (1996) for small angle misalignment. In the scenario they studied, Lense-Thirring precession is taken into account causing the accretion disc to warp as the black hole forces a realignment of the innermost part of the accretion disc. The warping radius is the radius where the Lense-Thirring effect becomes negligible. The realignment occurs within 3×10^8 years for a $10^9 M_{\odot}$ black hole, for an accretion rate of $1 M_{\odot} \text{ yr}^{-1}$ and a warping radius of 100 Schwarzschild radii. This timescale is probably a good estimate for Cygnus A. Considering that the age for the jet that we derive from the precession model is much less than 10^8 years, this model is certainly possible from the observations.

4.4.2 Companion black hole

Another possible mechanism for precession is a companion black hole. As the companion black hole will exert a torque on the accretion disc, and thereby misalign it with the primary black hole spin, the resulting precession is similar as described in the above section. This mechanism is used to explain precession in microquasar jets and pre-main sequence star jets, albeit with the companion then being an unknown star instead of a black hole. Canalizo et al. (2003) did detect a possible second nucleus with the Keck, at a distance of $0.4''$ or ~ 400 pc from the jet ejecting or primary black hole. Considering that there is a molecular cloud (Bellamy & Tadhunter 2004) and a possible companion nucleus (Canalizo et al. 2003), both causes (infalling gas which causes the accretion disc to be misaligned and a companion black hole that causes the accretion disc to be misaligned) are possibly at work in Cygnus A.

4.4.3 Angular momentum disc and host galaxy

A third possible mechanism for driving the precession is an offset in angular momentum vector direction between the angular momentum in the accretion disc and the angular momentum of the gas in the host galaxy. In this case the gas in the host galaxy will torque the accretion disc, thereby causing precession, as well as causing a misalignment of the accretion disc angular momentum and that of the super-massive black hole.

4.5 Independent estimates of jet speeds: from jet knots distances

Under certain assumptions one can calculate the jet speed from the observed distances from the core for the knots in the jet and comparing these with the distances for the knots in the counterjet. A first assumption is that corresponding knots on the jet and counterjet side were emitted at the same time, and therefore are not shocks along the path of the jet due to environmental differences. The assumption is minimised for the inner jets, however, as the emission from the inner jet is very weak, it is not possible to derive a reliable jet speed just from the inner jet. The second assumption is that the knots were emitted with the same speed in anti-parallel directions, and have a similar deceleration/acceleration along their paths; i.e. that there are no environmental differences between the two sides. To be able to measure these distances, i.e. take out the effect of projection, one needs to know the inclination angle of the jet with respect to our line of sight, θ . We find this angle to be 60° from

Table 1. Jet speeds derived from plausible matchings of different pairs of knots from the jet and counterjet. As fewer knots are observed in the counterjet there is no unique pairing. We use an inclination angle of 60° in calculating the jet speed. The labels for the knots correspond to those in Figs. 2 to 6.

jet knot	counterjet knot	β
W4	E1	0.16
W7	E2	0.27
W9	E3	0.21
W10	E3	0.26
W12	E4	0.22
W12	E5	0.19

our precession modelling (Sec. 4.1). Finally there is a more practical problem, the knots on the counterjet side are much weaker, hence we do not detect as many knots on the counterjet side as we do on the jet side. This leads to some uncertainty about how the knots should be paired. Bearing all these caveats in mind we find the jet speed, β , using:

$$\beta \cos \theta = \left(\frac{x-1}{x+1} \right) \quad (1)$$

where x is the distance between the core and a knot in the jet divided by the distance between the core and corresponding knot in the counterjet.

Table 1 lists the jet speeds for those knots that we assessed as being plausible pairs. The extreme (but formally allowed) values for jet speed for any pairing were $0.98c$ (knot W7 and E1) and $0.07c$ (knots W12 and E6). Note that several jet knots can be paired plausibly with more than one counterjet knot, and indeed, several counterjet knots can be paired with more than one jet knot. This gives a clear indication of the uncertainty in pairing the knots. The inference from Table 1 is that the jet speeds are fairly slow, lower than the best fit jet speed derived from our precession model.

4.6 Jet speeds for Cygnus A from the literature

Krichbaum et al. (1998) use two epochs of 22-GHz VLBI data to determine the jet speed for Cygnus A from the proper motion of the knots observed, as well as from the difference in luminosity between the jet and counterjet. From the observed proper motion of knots in the jet they derive an apparent jet speed of less than $0.27c$ (recalculated for the Hubble constant we assume throughout this paper) and an inclination angle of less than 50° . Krichbaum et al. (1998) determined the jet-to-counterjet ratio near the nucleus to be 1.3 although the steeper spectrum of the pc-scale counterjet compared with the pc-scale jet suggests that this side is being absorbed so this number is an upper limit and may be closer to unity. Using this flux ratio between the jet and the counterjet, and not taking light-travel time effects into account, they derive jet speeds between $0.27c$ and $0.82c$. However, Krichbaum et al. (1998) assert that the low jet speeds 'are too low to be considered realistic for Cygnus A'. Sorathia et al. (1996) used the same methods with VLBA and VLBI observations to derive a jet speed between $0.5c$ and $0.8c$ for an inclination angle to the line of sight between 45° and 75° , again assuming a Hubble parameter of $73 \text{ km s}^{-1} \text{ Mpc}^{-1}$.

Carilli et al. (1996) measured the flux ratio to be between 5 and 21 for the pc-scale jet (using VLBI data) and 2.6 ± 1 for the kpc-scale jet, but don't derive a jet speed for the kpc jet. However, Pelletier & Roland (1986) derive an upper limit to the jet speed of

Table 2. The table lists the literature values for jet speeds derived assuming a precession model and the relevant reference.

source	jet speed β	reference
3C 388	0.15	Gower et al. (1982)
NGC 326	0.20	Gower et al. (1982)
4C29.47	≤ 0.2	Condon & Mitchell (1984)
PKS 2300-18	≤ 0.3	Hunstead et al. (1984)

$0.6c$ in Cygnus A, using hydrodynamical modelling of the jets and the shock conditions in the hotspots.

Therefore, the range of jet speeds we derive for the kpc-scale jet, which has potentially undergone deceleration, is not unrealistic, compared to previously measured jet speed for the pc-scale jet and the modelled value for the kpc-scale jet.

4.7 Comparison of jet speed with other precessing AGN

In the literature compilation of precessing sources plotted in Fig. 11 there were 5 AGN. For 4 of these the authors gave the jet speed (or upper limit) derived from fitting a precessing jet model. These jet speeds are listed in Table 2. Interestingly, in all 4 cases the jet speed was constrained to be less than $0.3c$. Therefore, it seems reasonable that we find a jet speed of similar magnitude in Cygnus A.

4.8 Wardle & Aaron's study

Wardle & Aaron (1997) studied the jet to counterjet luminosity ratio for the 13 3CR sources with deep VLA images made by Bridle et al. (1994). To exclude possible effects from interaction with lobe material, they studied only the inner, straight kpc-scale jets. Wardle & Aaron assumed a spectral index of 0.6, and that the flux density enhancement is D^δ with D the Doppler factor and $\delta = 2.6$ appropriate for a continuous emission model of the jet. Wardle & Aaron (1997) conclude from the measured luminosity ratio that the jet speeds for the kpc-scale jets are between $0.6c$ – $0.7c$, and that the intrinsic asymmetry in the jets is small.

The analysis by Wardle & Aaron (1997) is statistical, as the inclination angles are unknown, and they admit that their sample is biased towards the largest sources. Considering the statistical analysis is over a biased sample, we see no reason to shy away from considering slow jet speeds for the kpc-scale jet in Cygnus A.

5 CONCLUSIONS

We have examined the detailed structure of the radio jet and counterjet in multi-band, multi-VLA configuration radio images kindly supplied by C. Carilli.

The trace of the radio knots that delineate the jet and counterjet deviates from a straight line, at least part of which can be satisfactorily fitted with the precession model of Hjellming & Johnston (1981). We find plausible parameter values for the precession model fits with jet speeds $\lesssim 0.5c$, which are consistent with independent methods of estimating the jet speed in Cygnus A.

The fact we observe precession in AGN seems to indicate that the jet is launched from the accretion disc. Comparing precession periods for sources with different masses, we find that young stellar objects have longer periods than microquasars, but that AGN have the longest periods.

ACKNOWLEDGEMENTS

KCS would like to thank St John's College, Oxford for a fellowship and John Everett for several discussions relating to the work presented in this paper. KMB expresses her gratitude to the Royal Society and both authors thank especially Chris Carilli for providing the radio data analysed in this paper and Robert Laing for helpful discussion. We are very grateful to the referee for helpful comments.

REFERENCES

- Bellamy M. J., Tadhunter C. N., 2004, MNRAS, 353, 105
 Blundell K. M., Bowler M. G., 2004, ApJL, 616, L159
 Bridle A. H., Hough D. H., Lonsdale C. J., Burns J. O., Laing R. A., 1994, AJ, 108, 766
 Canalizo G., Max C., Whysong D., Antonucci R., Dahm S. E., 2003, ApJ, 597, 823
 Carilli C., Perley R., Bartel N., Dreher J., 1996, The jets in Cygnus A: from pc- to kpc-scales. Cygnus A – Study of a Radio Galaxy, pp 76–+
 Carilli C. L., Perley R. A., Dreher J. W., Leahy J. P., 1991, ApJ, 383, 554
 Condon J. J., Mitchell K. J., 1984, ApJ, 276, 472
 Conway J. E., Blanco P. R., 1995, ApJL, 449, L131+
 Crocker M. M., Davis R. J., Spencer R. E., Eyres S. P. S., Bode M. F., Skopal A., 2002, MNRAS, 335, 1100
 Eilek J. A., Burns J. O., Odea C. P., Owen F. N., 1984, ApJ, 278, 37
 Gower A. C., Gregory P. C., Unruh W. G., Hutchings J. B., 1982, ApJ, 262, 478
 Hjellming R. M., Johnston K. J., 1981, ApJL, 246, L141
 Hunstead R. W., Murdoch H. S., Condon J. J., Phillips M. M., 1984, MNRAS, 207, 55
 Kaastra J. S., Roos N., 1992, A&A, 254, 96
 Krichbaum T. P., Alef W., Witzel A., Zensus J. A., Booth R. S., Greve A., Rogers A. E. E., 1998, A&A, 329, 873
 Ledlow M. J., Owen F. N., Miller N. A., 2005, AJ, 130, 47
 Lobanov A. P., Roland J., 2005, A&A, 431, 831
 Miller-Jones J. C. A., Blundell K. M., Rupen M. P., Mioduszewski A. J., Duffy P., Beasley A. J., 2004, ApJ, 600, 368
 Mioduszewski A. J., Rupen M. P., Hjellming R. M., Pooley G. G., Waltman E. B., 2001, ApJ, 553, 766
 Muxlow T. W. B., Jullian M., Linfield R., 1984, in Fanti R., Kellermann K. I., Setti G., eds, VLBI and Compact Radio Sources Vol. 110 of IAU Symposium, The Radio Jet in 3C418. pp 141–+
 Nair S., Jin C., Garrett M. A., 2005, MNRAS, 362, 1157
 Owen F. N., Ledlow M. J., Morrison G. E., Hill J. M., 1997, ApJL, 488, L15+
 Pelletier G., Roland J., 1986, A&A, 163, 9
 Perley R. A., Carilli C. L., 1996, The structure and polarization of Cygnus A at λ 3.6cm. Cygnus A – Study of a Radio Galaxy, pp 168–+
 Sahai R., Le Mignant D., Sánchez Contreras C., Campbell R. D., Chaffee F. H., 2005, ApJL, 622, L53
 Scheuer P. A. G., 1982, in Heeschen D. S., Wade C. M., eds, Extragalactic Radio Sources Vol. 97 of IAU Symposium, Morphology and power of radio sources. pp 163–165
 Scheuer P. A. G., Feiler R., 1996, MNRAS, 282, 291
 Sorathia B., Bartel N., Beitenholz M., Carilli C., 1996, The parsec-scale jet and counterjet in Cygnus A. Cygnus A – Study of a Radio Galaxy, pp 86–+
- Steenbrugge K. C., Blundell K. M., 2007, Ap&SS, 310, 321
 Steenbrugge K. C., Blundell K. M., P. D., 2008, submitted, MNRAS
 Tadhunter C., Marconi A., Axon D., Wills K., Robinson T. G., Jackson N., 2003, MNRAS, 342, 861
 Vlemmings W. H. T., Diamond P. J., Imai H., 2006, Nature, 440, 58
 Wardle J. F. C., Aaron S. E., 1997, MNRAS, 286, 425
 Wirth A., Smarr L., Gallagher J. S., 1982, AJ, 87, 602
 Woo J.-H., Urry C. M., 2002, ApJ, 579, 530
 Wu X.-B., Liu F. K., 2004, ApJ, 614, 91